Transp Porous Med (2013) 99:467–491
DOI 10.1007/s11242-013-0196-0

Traveling Wave Solutions in a Generalized Theory for Macroscopic Capillarity

O. Hönig · F. Doster · R. Hilfer

Received: 20 December 2012 / Accepted: 11 June 2013 / Published online: 28 June 2013

Abstract One-dimensional traveling wave solutions for imbibition processes into a homogeneous porous medium are found within a recent generalized theory of macroscopic capillarity. The generalized theory is based on the hydrodynamic differences between percolating and nonpercolating fluid parts. The traveling wave solutions are obtained using a dynamical systems approach. An exhaustive study of all smooth traveling wave solutions for primary and secondary imbibition processes is reported here. It is made possible by introducing two novel methods of reduced graphical representation. In the first method the integration constant of the dynamical system is related graphically to the boundary data and the wave velocity. In the second representation the wave velocity is plotted as a function of the boundary data. Each of these two graphical representations provides an exhaustive overview over all one-dimensional and smooth solutions of traveling wave type, that can arise in primary and secondary imbibition. Analogous representations are possible for other systems, solution classes, and processes.

Keywords Traveling waves · Capillarity · Multiphase flow · Porous media

1 Introduction

Almost all accepted and applied theories of multiphase flow in porous media are based on generalized Darcy laws and the concurrent concept of relative permeabilities

O. Hönig · R. Hilfer
ICP, University of Stuttgart, Pfaffenwaldring 27, 70569 Stuttgart, Germany
e-mail: hilfer@ica1.uni-stuttgart.de

F. Doster
Department of Civil and Environmental Engineering, E-208 E-Quad,
Princeton University, Princeton, NJ 08544, USA

F. Doster (✉)
Department of Mathematics, University of Bergen, P. O. Box 7800,
5020 Bergen, Norway
e-mail: fdoster@princeton.edu

(Wyckoff and Botset 1936). Despite the fact that (Wyckoff and Botset 1936) strongly emphasized the variation of hydraulically disconnected fluid regions (Jamin 1860), almost all subsequent applications of the relative permeability concept treat the residual nonwetting (or irreducible wetting) saturations as material constants (Bear 1972; Collins 1961; Dullien 1992; Helmig 1997; Wiest 1969; Scheidegger 1957; Marsily 1986). Modern theories of multiphase flow in porous media often resort to microscopic models (e.g., network models) (Bear et al. 1987; Bryant and Blunt 1992; Dias and Payatakes 1986; Dijke and Sorbie 2002; Ferer et al. 2004) in an attempt to derive or estimate macroscopic relative permeabilities from pore scale parameters. It was emphasized in Wyckoff and Botset (1936), however, that the possibility of determining the overall dynamical behavior of nonhomogeneous fluids from a study of microscopic details is remote (Wyckoff and Botset 1936, p. 326).

Experimentally, the volume fraction of stationary, locked, trapped, or nonpercolating fluid phases varies strongly with time and position (Abrams 1975; Avraam and Payatakes 1995; Taber 1969; Wyckoff and Botset 1936). Dispersed droplets, bubbles, or ganglia of one fluid phase obstruct the motion of the other fluid phase. Extensive experimental and theoretical studies of this simple phenomenon exist (Avraam and Payatakes 1999; Jamin 1860). Theoretically, the fundamental difference between trapped percolating and mobile nonpercolating fluid parts was first introduced in Hilfer (1998, 2006a,b,c) and the resulting mathematical model was partially explored further in Hilfer and Doster (2010), Doster and Hilfer (2011), Doster (2011), Doster et al. (2010, 2012).

The objective of this paper is twofold: firstly, the paper finds traveling wave solutions for the model introduced in Hilfer (2006a,b,c). While some approximate analytical and numerical solutions of the theory have been found in Hilfer (2006a,b,c), Hilfer and Doster (2010), Doster et al. (2010), Doster (2011), Doster and Hilfer (2011); Doster et al. (2012) the existence of traveling waves for this system has remained an open question and is analyzed here for the first time. This paper reports the existence of traveling waves for the generalized theory under the assumption that the nonpercolating phases are immobile. The second objective of this paper is to introduce two novel graphical representations of the solution space, that give a complete and exhaustive overview of all traveling wave solutions, that are infinitely often differentiable. Both representations are based on transforming the boundary value problem for the nonlinear partial differential equations to a dynamical system. The first representation is based on the integration constant of the dynamical system related to the boundary data and the wave velocity. The second representation is based on the wave velocity as a function of boundary data.

A word on notation: Throughout the paper, variables with a hat ˆ have a physical dimension and all others are dimensionless, e.g. the time $\hat{t}$ has the dimension of seconds "s", while t is dimensionless.

2 Formulation of the Model

In the first part of this section, we give a brief description of the model. For physical details and motivation of constitutive assumptions we refer to the previously published works Hilfer (2006a,b,c). In the second part, problem-specific assumptions are given and a dimensionless fractional flow formulation is derived.

2.1 The Generalized Model

A one-dimensional, horizontal, homogeneous, isotropic, and rigid porous column filled with two immiscible Newtonian fluids is considered here. The water phase denoted as $\mathbb{W}$ with

saturation $S_{\mathbb{W}}$ consists of percolating S_1 and nonpercolating water S_2. The oil phase denoted as $\mathbb{O}$ with saturation $S_{\mathbb{O}}$ consists of percolating oil S_3 and nonpercolating oil S_4. A region occupied by fluid is called percolating if it is path-connected to the boundary of the sample. For a more precise definition see Hilfer (2006b). All saturations are functions of one-dimensional position $\hat{x}$ and time $\hat{t} \in \mathbb{R}^+$. Throughout the paper we idealize a large but finite system as infinitely extended so that $\hat{x} \in \mathbb{R}$ holds. Variables with a hat ˆ have a physical dimension. The volume fraction of the i-th phase is $\phi_i = \phi_i(\hat{x}, \hat{t}) = \phi(\hat{x}, \hat{t}) S_i(\hat{x}, \hat{t})$ and the volume fraction of the porous medium is $\phi_5 = \phi_5(\hat{x}, \hat{t}) = 1 - \phi(\hat{x}, \hat{t})$ where the porosity $\phi = \phi(\hat{x}, \hat{t})$ is defined as the volume fraction of the pore space.

2.1.1 Balance Laws

Volume conservation for incompressible fluids and an incompressible porous medium requires

$$S_1 + S_2 + S_3 + S_4 = 1, \tag{1a}$$

$$\phi_1 + \phi_2 + \phi_3 + \phi_4 + \phi_5 = 1. \tag{1b}$$

The mass balance for phase $i \in \{1, 2, 3, 4\}$ reads in differential form

$$\partial_{\hat{t}} \left(\phi_i \hat{\varrho}_i \right) + \partial_{\hat{x}} \left(\phi_i \hat{\varrho}_i \hat{v}_i \right) = \hat{M}_i, \tag{2}$$

where $\hat{\varrho}_i = \hat{\varrho}_i(\hat{x}, \hat{t})$ and $\hat{v}_i = \hat{v}_i(\hat{x}, \hat{t})$ are the density and the velocity of the i-th phase. $\hat{M}_i$ is the mass transfer rate from all other phases into phase i.

The momentum balance for phase $i \in \{1, 2, 3, 4\}$ is written as

$$\phi_i \hat{\varrho}_i \mathrm{D}^i_{\hat{t}} \hat{v}_i - \phi_i \partial_{\hat{x}} \hat{\Sigma}_i - \phi_i \hat{F} = \hat{m}_i - \hat{v}_i \hat{M}_i, \tag{3}$$

where $\hat{\Sigma}_i$ is the stress tensor in the ith phase, $\hat{F}_i$ is the body force per unit volume acting on the ith phase, $\hat{m}_i$ is the momentum transfer into phase i from all the other phases, and $\mathrm{D}^i_{\hat{t}} = \mathrm{D}^i / \mathrm{D}_{\hat{t}} = \partial_{\hat{t}} + \hat{v}_i \partial_{\hat{x}}$ denotes the material derivative for phase i. The inertia can be neglected

$$\mathrm{D}^i_{\hat{t}} \hat{v}_i = 0 \tag{4}$$

for sufficient small Reynolds numbers.

2.1.2 Constitutive Assumptions

The porous medium is macroscopically homogeneous

$$\phi(\hat{x}, \hat{t}) = \phi \tag{5}$$

and the fluids are incompressible

$$\hat{\varrho}_1(\hat{x}, \hat{t}) = \hat{\varrho}_{\mathbb{W}}, \tag{6a}$$

$$\hat{\varrho}_2(\hat{x}, \hat{t}) = \hat{\varrho}_{\mathbb{W}}, \tag{6b}$$

$$\hat{\varrho}_3(\hat{x}, \hat{t}) = \hat{\varrho}_{\mathbb{O}}, \tag{6c}$$

$$\hat{\varrho}_4(\hat{x}, \hat{t}) = \hat{\varrho}_{\mathbb{O}}. \tag{6d}$$

The percolating and the nonpercolating phases are able to exchange mass through breakup and coalescence of droplets, ganglia and clusters. The mass transfer rates must depend on rates of saturation change. Here, they are assumed to be

$$\hat{M}_1 = -\hat{M}_2 = \eta_2 \phi \hat{\varrho}_{\mathbb{W}} \left(\frac{S_2 - S_2^*}{S_{\mathbb{W}}^* - S_{\mathbb{W}}} \right) \partial_{\hat{t}} S_{\mathbb{W}}, \tag{7a}$$

$$\hat{M}_3 = -\hat{M}_4 = \eta_4 \phi \hat{\varrho}_{\mathbb{O}} \left(\frac{S_4 - S_4^*}{S_{\mathbb{O}}^* - S_{\mathbb{O}}} \right) \partial_{\hat{t}} S_{\mathbb{O}}, \tag{7b}$$

where η_2, η_4 are constants. The mass exchange has to change sign with the rate of saturation change (see Hilfer (2006a,b,c) for more details). The quantities S_2^*, S_4^*, $S_{\mathbb{W}}^*$, $S_{\mathbb{O}}^*$ are defined by

$$S_2^* = S_{\mathbb{W}\,\mathrm{dr}}(1 - \Theta(\partial_{\hat{t}} S_{\mathbb{W}})), \tag{8a}$$

$$S_4^* = S_{\mathbb{O}\,\mathrm{im}}(1 - \Theta(\partial_{\hat{t}} S_{\mathbb{O}})), \tag{8b}$$

$$S_{\mathbb{W}}^* = (1 - S_{\mathbb{O}\,\mathrm{im}})\Theta(\partial_{\hat{t}} S_{\mathbb{W}}) + S_{\mathbb{W}\,\mathrm{dr}}(1 - \Theta(\partial_{\hat{t}} S_{\mathbb{W}})), \tag{8c}$$

$$S_{\mathbb{O}}^* = 1 - S_{\mathbb{W}}^* = S_{\mathbb{O}\,\mathrm{im}}(1 - \Theta(\partial_{\hat{t}} S_{\mathbb{O}})) + (1 - S_{\mathbb{W}\,\mathrm{dr}})\Theta(\partial_{\hat{t}} S_{\mathbb{O}}), \tag{8d}$$

where $S_{\mathbb{W}\,\mathrm{dr}}$, $S_{\mathbb{O}\,\mathrm{im}}$ are limiting saturations for S_2, S_4. The Heaviside unit step function $\Theta(x)$ is introduced as

$$\Theta(x) = \frac{1}{2}(\mathrm{sgn}(x) + 1) = \begin{cases} 0 & \text{for} \quad x < 0, \\ \dfrac{1}{2} & \text{for} \quad x = 0, \\ 1 & \text{for} \quad x > 0. \end{cases} \tag{9}$$

The stress tensor for the four phases are specified as

$$\hat{\Sigma}_1 = -\hat{P}_1, \tag{10a}$$

$$\hat{\Sigma}_2 = -\hat{P}_3 + \gamma \hat{P}_2^* {S_2}^{\gamma - 1}, \tag{10b}$$

$$\hat{\Sigma}_3 = -\hat{P}_3, \tag{10c}$$

$$\hat{\Sigma}_4 = -\hat{P}_1 + \delta \hat{P}_4^* {S_4}^{\delta - 1}, \tag{10d}$$

where $\hat{P}_2^*$, $\hat{P}_4^*$, γ, δ are constants and $\hat{P}_1$, $\hat{P}_3$ are the fluid pressures in the percolating phases. The additional terms account for the energy density stored fluid–fluid interfaces [see Hilfer (2006a,b,c) for more details]. The body forces are assumed to be given by capillarity. They are specified as

$$\hat{F}_1 = 0, \tag{11a}$$

$$\hat{F}_2 = \hat{\Pi}_{\mathrm{a}}^* \partial_{\hat{x}} {S_1}^{-\alpha}, \tag{11b}$$

$$\hat{F}_3 = 0, \tag{11c}$$

$$\hat{F}_4 = \hat{\Pi}_{\mathrm{b}}^* \partial_{\hat{x}} {S_3}^{-\beta}, \tag{11d}$$

where $\hat{\Pi}_{\mathrm{a}}^*$, $\hat{\Pi}_{\mathrm{b}}^*$, α, β are constants. The additional terms represent capillary body forces acting on non-percolating phases [see Hilfer (2006a,b,c) for more details]. Finally, the momentum transfer terms are assumed to be given by linear viscous drag characterized by constitutive resistance coefficients $\hat{R}_{ij}$ through the equations

$$\hat{m}_1 = \hat{R}_{13}(\hat{v}_3 - \hat{v}_1) + \hat{R}_{14}(\hat{v}_4 - \hat{v}_1) - \hat{R}_{15}\hat{v}_1, \tag{12a}$$
$$\hat{m}_2 = \hat{R}_{23}(\hat{v}_3 - \hat{v}_2) + \hat{R}_{24}(\hat{v}_4 - \hat{v}_2) - \hat{R}_{25}\hat{v}_2, \tag{12b}$$
$$\hat{m}_3 = \hat{R}_{31}(\hat{v}_1 - \hat{v}_3) + \hat{R}_{32}(\hat{v}_2 - \hat{v}_3) - \hat{R}_{35}\hat{v}_3, \tag{12c}$$
$$\hat{m}_4 = \hat{R}_{41}(\hat{v}_1 - \hat{v}_4) + \hat{R}_{42}(\hat{v}_2 - \hat{v}_4) - \hat{R}_{45}\hat{v}_4, \tag{12d}$$

where $\hat{R}_{12} = \hat{R}_{34} = 0$ was already used because there is no common interface and hence, no direct viscous interaction between these phase pairs.

2.1.3 Reformulation

The balance laws (1),(2), and (3) are arranged in terms of volume flux densities. Inserting Eq. (4) into Eq. (3), it becomes linear in the velocities $\hat{v}_i$. Using Eqs. (7), (12) the right hand side of Eq. (3) can be written as

$$\begin{pmatrix} \hat{m}_1 - \hat{M}_1\hat{v}_1 \\ \hat{m}_2 + \hat{M}_1\hat{v}_2 \\ \hat{m}_3 - \hat{M}_3\hat{v}_3 \\ \hat{m}_4 + \hat{M}_3\hat{v}_4 \end{pmatrix} = -\hat{R} \begin{pmatrix} \hat{v}_1 \\ \hat{v}_2 \\ \hat{v}_3 \\ \hat{v}_4 \end{pmatrix}, \tag{13}$$

where the components of the generalized resistance matrix $\hat{R}$ are

$$\hat{R}(S_{\mathbb{W}}, S_2, S_4, \partial_{\hat{t}} S_{\mathbb{W}}) = \begin{pmatrix} \hat{R}_{11} & 0 & -\hat{R}_{13} & -\hat{R}_{14} \\ 0 & \hat{R}_{22} & -\hat{R}_{23} & -\hat{R}_{24} \\ -\hat{R}_{31} & -\hat{R}_{32} & \hat{R}_{33} & 0 \\ -\hat{R}_{41} & -\hat{R}_{42} & 0 & \hat{R}_{44} \end{pmatrix} \tag{14}$$

and the shorthand notation

$$\hat{R}_{11}(S_{\mathbb{W}}, S_2, \partial_{\hat{t}} S_{\mathbb{W}}) = \hat{R}_{15} + \hat{R}_{13} + \hat{R}_{14} + \hat{M}_1, \tag{15a}$$
$$\hat{R}_{22}(S_{\mathbb{W}}, S_2, \partial_{\hat{t}} S_{\mathbb{W}}) = \hat{R}_{25} + \hat{R}_{23} + \hat{R}_{24} - \hat{M}_1, \tag{15b}$$
$$\hat{R}_{33}(S_{\mathbb{W}}, S_4, \partial_{\hat{t}} S_{\mathbb{W}}) = \hat{R}_{35} + \hat{R}_{31} + \hat{R}_{32} + \hat{M}_3, \tag{15c}$$
$$\hat{R}_{44}(S_{\mathbb{W}}, S_4, \partial_{\hat{t}} S_{\mathbb{W}}) = \hat{R}_{45} + \hat{R}_{41} + \hat{R}_{42} - \hat{M}_3 \tag{15d}$$

was used. To obtain expressions for the volume flux densities, Eq. (13) is inserted into Eq. (1). The resulting set of equations is solved for the velocities and multiplied with the corresponding phase volume fractions ϕ_i. As a result one finds

$$\begin{pmatrix} \hat{q}_1 \\ \hat{q}_2 \\ \hat{q}_3 \\ \hat{q}_4 \end{pmatrix} = \begin{pmatrix} \phi_1\hat{v}_1 \\ \phi_2\hat{v}_2 \\ \phi_3\hat{v}_3 \\ \phi_4\hat{v}_4 \end{pmatrix} = \hat{\Lambda} \begin{pmatrix} \partial_{\hat{x}}\hat{\Sigma}_1 + \hat{F}_1 \\ \partial_{\hat{x}}\hat{\Sigma}_2 + \hat{F}_2 \\ \partial_{\hat{x}}\hat{\Sigma}_3 + \hat{F}_3 \\ \partial_{\hat{x}}\hat{\Sigma}_4 + \hat{F}_4 \end{pmatrix}, \tag{16}$$

where the mobility matrix $\hat{\Lambda}$ with components

$$\hat{\lambda}_{ij}(S_{\mathbb{W}}, S_2, S_4, \partial_{\hat{t}} S_{\mathbb{W}}) = \phi^2 S_i S_j \hat{R}_{ij}^{-1} \tag{17}$$

has been introduced.

The mass balances and the momentum balances are expressed in terms of the primary variables $S_{\mathbb{W}}$, S_2, S_4. A linear combination and accounting for the volume conservation yields for $\hat{t} \in \mathbb{R}^+$ and $\hat{x} \in \mathbb{R}$

$$\phi \frac{\partial}{\partial \hat{t}} S_{\mathbb{W}} = -\frac{\partial}{\partial \hat{x}} \hat{q}_{\mathbb{W}}, \tag{18a}$$

$$\phi \frac{\partial}{\partial \hat{t}} S_2 = -\frac{\hat{M}_1}{\hat{\varrho}_{\mathbb{W}}} - \frac{\partial}{\partial \hat{x}} \hat{q}_2, \tag{18b}$$

$$\phi \frac{\partial}{\partial \hat{t}} S_4 = -\frac{\hat{M}_3}{\hat{\varrho}_{\mathbb{O}}} - \frac{\partial}{\partial \hat{x}} \hat{q}_4, \tag{18c}$$

$$\frac{\partial}{\partial \hat{x}} (\hat{q}_{\mathbb{W}} + \hat{q}_{\mathbb{O}}) = 0, \tag{18d}$$

where the total water flux formed by the percolating and the nonpercolating water flux is denoted by $\hat{q}_{\mathbb{W}} = \hat{q}_1 + \hat{q}_2$. Similarly the oil flux is denoted by $\hat{q}_{\mathbb{O}} = \hat{q}_3 + \hat{q}_4$. Initial and boundary conditions are given below.

2.1.4 Self-Consistence Closure Condition

The system of nonlinear partial differential equations is closed self-consistently. The most general form of self-consistent closure was given in Hilfer and Doster (2010). Here, a simplification is employed. Guided by the residual decoupling approximation (Hilfer 2006b) the relation

$$\partial_{\hat{x}} \hat{P}_3 = \partial_{\hat{x}} \hat{P}_1 + \frac{1}{2} \partial_{\hat{x}} \left(\hat{\Pi}_{\mathrm{a}}^* {S_1}^{-\alpha} - \hat{\Pi}_{\mathrm{b}}^* {S_3}^{-\beta} + \gamma \hat{P}_2^* {S_2}^{\gamma-1} - \delta \hat{P}_4^* {S_4}^{\delta-1} \right) \tag{19}$$

suffices to recover the traditional capillary pressure concept for sufficiently slow displacement processes from the generalized theory. The difference between the phase pressures of the percolating phases

$$\hat{P}_{\mathrm{c}} := \hat{P}_3 - \hat{P}_1 \tag{20}$$

is identified as the macroscopic capillary pressure. Integrating Eq. (19) yields

$$\hat{P}_{\mathrm{c}}(S_1, S_2, S_3, S_4) = \frac{1}{2} \left(\Pi_{\mathrm{a}}^* {S_1}^{-\alpha} - \Pi_{\mathrm{b}}^* {S_3}^{-\beta} + \gamma P_2^* {S_2}^{\gamma-1} - \delta P_4^* {S_4}^{\delta-1} \right) + \hat{P}_0^*, \tag{21}$$

where the integration constant $\hat{P}_0^*$ is determined experimentally together with the parameters $\hat{\Pi}_{\mathrm{a}}^*$, $\hat{\Pi}_{\mathrm{b}}^*$, $\hat{P}_2^*$, $\hat{P}_4^*$ and the exponents $\alpha, \beta, \gamma, \delta$.

2.2 Problem-Specific Assumptions

2.2.1 Boundary and Initial Conditions

A time-independent total flux $q_{\mathrm{tot}} = q_{\mathbb{W}} + q_{\mathbb{O}}$ is applied on the left hand side of the porous medium. The total flux is also independent of position due to the incompressibility of the fluids. Hence, the total flux is a constant

$$q_{\mathrm{tot}}(\hat{x}, \hat{t}) = q_{\mathrm{tot}} = \mathrm{const.} \tag{22}$$

for all $\hat{x} \in \mathbb{R}$ and $\hat{t} > 0$. The saturations are

$$S_i(-\infty, \hat{t}) = S_i^{\mathrm{l}} \quad i \in \{\mathbb{W}, \mathbb{O}, 2, 4\}, \tag{23a}$$

$$S_i(\infty, \hat{t}) = S_i^{\mathrm{r}} \quad i \in \{\mathbb{W}, \mathbb{O}, 2, 4\} \tag{23b}$$

for all times $\hat{t} \geq 0$ where the parameters S_i^{l}, S_i^{r} are constants. The initial conditions for Eq. (18) are

$$S_i(\hat{x}, 0) = S_i^0(\hat{x}) \quad i \in \{\mathbb{W}, \mathbb{O}, 2, 4\}, \tag{24}$$

where $S_i^0(\hat{x})$ is any continuous profile compatible with the limiting values in Eq. (23).

2.2.2 Viscous Drag Domination and Viscous Decoupling

Comparison with experiments suggests that the viscous coupling coefficients $\hat{R}_{ij}$ are typically of order $10^8 \mathrm{kgm}^{-3}\mathrm{s}^{-1}$ while the momentum transfer due to the mass exchange is only of order $\hat{M}_i \approx 10^3 \mathrm{kgm}^{-3}\mathrm{s}^{-1}$ (Doster and Hilfer 2011). Therefore it is assumed that the viscous drag with the wall dominates the momentum transfer

$$\hat{R}_{15} \gg \hat{M}_1, \tag{25a}$$
$$\hat{R}_{25} \gg \hat{M}_1, \tag{25b}$$
$$\hat{R}_{35} \gg \hat{M}_3, \tag{25c}$$
$$\hat{R}_{45} \gg \hat{M}_3. \tag{25d}$$

In addition, it is assumed that the viscous coupling between the phases and the porous medium is much larger than the viscous coupling between two phases

$$\hat{R}_{15} \gg \hat{R}_{ij}, \tag{26a}$$
$$\hat{R}_{25} \gg \hat{R}_{ij}, \tag{26b}$$
$$\hat{R}_{35} \gg \hat{R}_{ij}, \tag{26c}$$
$$\hat{R}_{45} \gg \hat{R}_{ij} \tag{26d}$$

for all pairs (i, j) with $i \in \{1, 2, 3, 4\}$ and $j \in \{1, 2, 3, 4, 5\}$ such that and $(i, j) \neq (2, 5)$ and $(i, j) \neq (4, 5)$. The assumptions lead to a constant resistance matrix $\hat{R}$, to immobile nonpercolating phases and to a mobility matrix $\hat{\Lambda}$ that has only λ_{11} and λ_{33} as nonzero components. These assumptions may be justified physically by the observation that the motion of contact lines on the internal surface requires to overcome capillary forces and this creates additional resistance that is much higher than the viscous drag.

2.2.3 Model Reduction and Dimensionless Fractional Flow Formulation

With the assumptions given in Eqs. (25), (26) the flow functions on the left hand side of Eq. (16) become

$$\hat{q}_{\mathbb{W}} = -\frac{\phi^2 (S_{\mathbb{W}} - S_2)^2}{\hat{R}_{11}} \frac{\partial}{\partial \hat{x}} \hat{P}_1, \tag{27a}$$
$$\hat{q}_{\mathbb{O}} = -\frac{\phi^2 (1 - S_{\mathbb{W}} - S_4)^2}{\hat{R}_{33}} \frac{\partial}{\partial \hat{x}} \hat{P}_3, \tag{27b}$$
$$\hat{q}_2 = 0, \tag{27c}$$
$$\hat{q}_4 = 0. \tag{27d}$$

These fluxes simplify the system of equations (18) significantly and permit an integration of the Eqs. (18b) and (18c) similar to Hilfer (2006b) to obtain explicit expressions for the nonpercolating phases

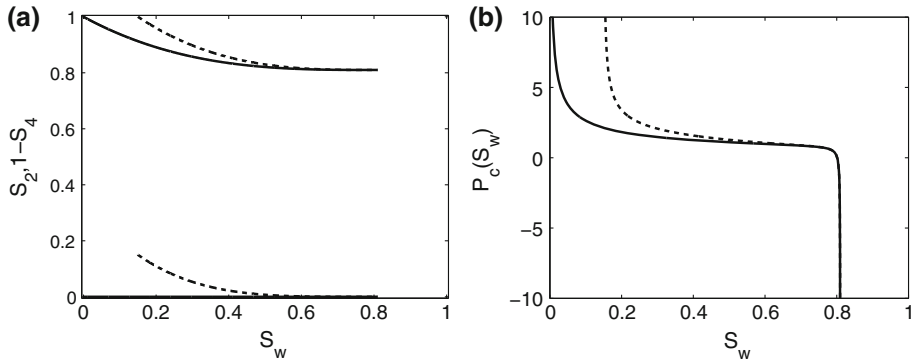

Fig. 1 Nonpercolating phases (**a**) as functions of water saturation from Eq. (28) and capillary pressure (**b**) from Eq. (29) with parameters from Tables 1 and 2 and $\hat{P}_0^* = 0$. *Solid lines* show primary imbibition, *dashed lines* show secondary imbibition. Both *curves* have to be read from left to right

$$S_2(S_{\mathbb{W}}; S_{20}, S_{\mathbb{W}0}) = S_2^* + (S_{20} - S_2^*)\left(\frac{S_{\mathbb{W}}^* - S_{\mathbb{W}}}{S_{\mathbb{W}}^* - S_{\mathbb{W}0}}\right)^{\eta_2}, \tag{28a}$$

$$S_4(S_{\mathbb{W}}; S_{40}, S_{\mathbb{W}0}) = S_4^* + (S_{40} - S_4^*)\left(\frac{S_{\mathbb{W}} - S_{\mathbb{W}}^*}{S_{\mathbb{W}0} - S_{\mathbb{W}}^*}\right)^{\eta_4} \tag{28b}$$

in terms of the water saturation and the initial data $(S_{20}, S_{40}, S_{\mathbb{W}0})$. Hence, also the capillary pressure becomes a function of water saturation and the initial data $(S_{20}, S_{40}, S_{\mathbb{W}0})$

$$\begin{aligned}\hat{P}_{\mathrm{c}}(S_{\mathbb{W}}; S_{20}, S_{40}, S_{\mathbb{W}0}) = \frac{1}{2}\big(&\Pi_{\mathrm{a}}^*(S_{\mathbb{W}} - S_2)^{-\alpha} - \Pi_{\mathrm{b}}^*(1 - S_{\mathbb{W}} - S_4)^{-\beta} \\ &+\gamma P_2^* S_2^{\gamma-1} - \delta P_4^* S_4^{\delta-1}\big) + \hat{P}_0^*,\end{aligned} \tag{29}$$

where the arguments of the functions $S_2(S_{\mathbb{W}}; S_{20}, S_{\mathbb{W}0})$ and $S_4(S_{\mathbb{W}}; S_{40}, S_{\mathbb{W}0})$ have been omitted for the sake of readability. Figure 1 shows the nonpercolating phases and the capillary pressure with respect to the water saturation using the parameters from Tables 1 and 2 and $\hat{P}_0^* = 0$. The figure shows that the nonpercolating phases and the capillary pressure almost coincide at a high saturation values.

To obtain a dimensionless form of Eq. (18a) we assume for a moment a large but finite system of length $\hat{l}$. Position, time, fluxes, and pressures are expressed in terms of the system

Table 1 Parameters for Eqs. (28), (29), (33), (34)

η_2	η_4	Π_{a}^*	Π_{b}^*	P_2^*	P_4^*	α	β	γ	δ	$S_{\mathbb{O}\,\mathrm{im}}$	$S_{\mathbb{W}\,\mathrm{dr}}$	$\frac{\hat{R}_{11}}{\hat{R}_{33}}$
4	3	1.6	0.025	2.5	0.4	0.52	0.9	1.5	3.5	0.19	0.15	2

Table 2 Limiting and initial saturations for primary and secondary imbibition

Parameter	S_2^*	S_4^*	$S_{\mathbb{W}}^*$	S_{20}	S_{40}	$S_{\mathbb{W}0}$
Primary	0	$S_{\mathbb{O}\,\mathrm{im}}$	$1 - S_{\mathbb{O}\,\mathrm{im}}$	0	0	0
Secondary	0	$S_{\mathbb{O}\,\mathrm{im}}$	$1 - S_{\mathbb{O}\,\mathrm{im}}$	$S_{\mathbb{W}\,\mathrm{dr}}$	0	$S_{\mathbb{W}\,\mathrm{dr}}$

length $\hat{l}$, a characteristic macroscopic velocity $\hat{u}$ and a characteristic pressure $\hat{P}_\mathrm{b}$, the breakthrough pressure which is defined as the inflection point of the capillary pressure curve. They are explicitly given by

$$\tilde{x} = \frac{1}{\hat{l}}\hat{x}, \tag{30a}$$

$$\tilde{t} = \frac{\hat{u}}{\hat{l}\phi}\hat{t}, \tag{30b}$$

$$q_i = \frac{1}{\phi^2\hat{u}}\hat{q}_i, \quad i \in \{\mathbb{W}, \mathbb{O}, 2, 4\}, \tag{30c}$$

$$P_i = \frac{1}{\hat{P}_\mathrm{b}}\hat{P}_i, \quad i \in \{1, 3, c\}. \tag{30d}$$

The dimensionless form of Eq. (18a) reads as

$$\frac{\partial}{\partial\tilde{t}}S_\mathbb{W} = \frac{1}{\mathrm{Ca}_\mathbb{W}}\frac{\partial}{\partial\tilde{x}}\left[(S_\mathbb{W} - S_2(S_\mathbb{W}))^2\frac{\partial}{\partial\tilde{x}}P_1\right], \tag{31}$$

where the macroscopic capillary number is defined as

$$\mathrm{Ca}_\mathbb{W} = \frac{\hat{R}_{11}\hat{u}\hat{l}}{\phi^2\hat{P}_\mathrm{b}}. \tag{32}$$

The capillary number gives the ratio of the macroscopic pressure drop and the macroscopic capillary pressure. It is identical to the macroscopic capillary number defined in Hilfer and Oeren (1996) if $\hat{R}_{11} = \hat{\mu}_\mathbb{W}/\phi^2\hat{k}$.

By defining a fractional flow function as in Doster and Hilfer (2011); Doster et al. (2012)

$$f(S_\mathbb{W}) = \frac{(S_\mathbb{W} - S_2(S_\mathbb{W}))^2}{(S_\mathbb{W} - S_2(S_\mathbb{W}))^2 + \frac{\hat{R}_{11}}{\hat{R}_{33}}(1 - S_\mathbb{W} - S_4(S_\mathbb{W}))^2} \tag{33}$$

and a capillary function

$$\mathrm{D}(S_\mathbb{W}) = -\frac{\hat{R}_{11}}{\hat{R}_{33}}\frac{(S_\mathbb{W} - S_2(S_\mathbb{W}))^2(1 - S_\mathbb{W} - S_4(S_\mathbb{W}))^2}{(S_\mathbb{W} - S_2(S_\mathbb{W}))^2 + \frac{\hat{R}_{11}}{\hat{R}_{33}}(1 - S_\mathbb{W} - S_4(S_\mathbb{W}))^2}\frac{\partial P_\mathrm{c}(S_\mathbb{W})}{\partial S_\mathbb{W}} \tag{34}$$

one gets

$$\frac{\partial S_\mathbb{W}}{\partial\tilde{t}} + \frac{q_\mathrm{tot}}{\mathrm{Ca}_\mathbb{W}}\frac{\partial f(S_\mathbb{W})}{\partial S_\mathbb{W}}\frac{\partial S_\mathbb{W}}{\partial\tilde{x}} - \frac{1}{\mathrm{Ca}_\mathbb{W}}\frac{\partial}{\partial\tilde{x}}\left[\mathrm{D}(S_\mathbb{W})\frac{\partial S_\mathbb{W}}{\partial\tilde{x}}\right] = 0. \tag{35}$$

Because we wish to have terms of equal magnitude in Eq. (35) we assume that $\hat{u}$ and $\hat{l}$ are such that

$$q_\mathrm{tot} = \mathrm{Ca}_\mathbb{W} \tag{36}$$

and position and time is again rescaled as

$$x = \mathrm{Ca}_\mathbb{W}\tilde{x}, \tag{37a}$$

$$t = \mathrm{Ca}_\mathbb{W}\tilde{t}. \tag{37b}$$

The result reads as

$$\frac{\partial S_\mathbb{W}}{\partial t} + \frac{\partial f(S_\mathbb{W})}{\partial S_\mathbb{W}}\frac{\partial S_\mathbb{W}}{\partial x} - \frac{\partial}{\partial x}\left[\mathrm{D}(S_\mathbb{W})\frac{\partial S_\mathbb{W}}{\partial x}\right] = 0. \tag{38}$$

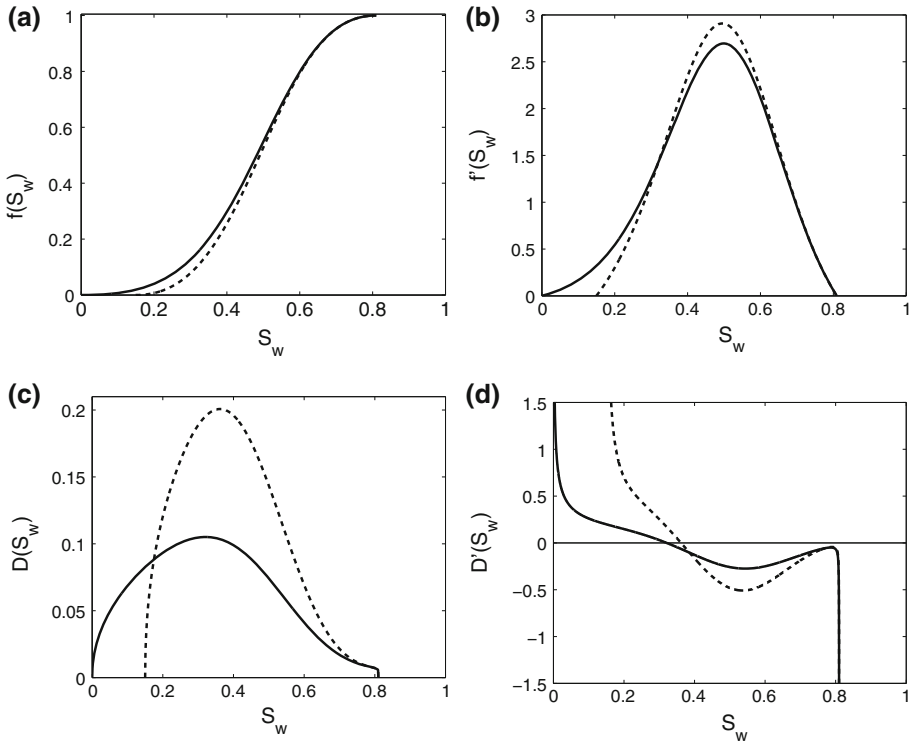

Fig. 2 Fractional flow function $f(S_{\mathbb{W}})$ (**a**), its derivative $f'(S_{\mathbb{W}})$ (**b**) and the capillary function $\mathrm{D}(S_{\mathbb{W}})$ (**c**) and its derivative $\mathrm{D}'(S_{\mathbb{W}})$ (**d**) for the parameters in Tables 1 and 2. The *solid line* shows the primary imbibition and the *dashed line* shows the secondary imbibition

Equation (38) has the same form as the dimensionless fractional flow formulation of the traditional model but the fractional flow function and the capillary function differ significantly.

We now return to the idealization that the sample is infinite such that $x \in \mathbb{R}$. The initial conditions defined in Eq. (24) read in dimensionless form as

$$S_i(\hat{x}, 0) = S_i^0(x) \quad i \in \{\mathbb{W}, \mathbb{O}, 2, 4\}, \tag{39}$$

for all $x \in \mathbb{R}$. The boundary conditions of (23) are in dimensionless form

$$S_i(-\infty, t) = S_i^{\mathrm{l}} \quad i \in \{\mathbb{W}, \mathbb{O}, 2, 4\}, \tag{40a}$$

$$S_i(\infty, t) = S_i^{\mathrm{r}} \quad i \in \{\mathbb{W}, \mathbb{O}, 2, 4\} \tag{40b}$$

for all times $t \geq 0$.

Figure 2 illustrates the fractional flow function $f(S_{\mathbb{W}})$, its derivative $f'(S_{\mathbb{W}})$ and the capillary function $\mathrm{D}(S_{\mathbb{W}})$ and its derivative $\mathrm{D}'(S_{\mathbb{W}})$ for the parameters in Tables 1 and 2. The solid lines show the primary imbibition and the dashed line show the secondary imbibition. The fractional flow function gives the ratio between the advective water flux and the advective total flux. Its value is higher for primary processes than for secondary processes. The derivative of the fractional flow function gives the velocity of the front. Its maximum value is higher for secondary imbibitions. The capillary functions show a maximum which is significantly

higher for the secondary processes. The derivatives of the capillary functions diverge in the limit where the water saturation goes to its maximal or minimal value.

3 Method of Solution

3.1 Traveling Wave Ansatz

In this section we transform the problem given by Eq. (38), the dimensionless boundary data (40) and the dimensionless initial data (39) into a system of ordinary differential equations. Following (Brevdo et al. 2001) similarity solutions of the form

$$S_{\mathrm{W}}(x,t) = S_{\mathrm{W}}(x-ct) = S_{\mathrm{W}}(y) \quad c = \text{const.} \tag{41}$$

are searched for. Inserting Eq. (41) into Eq. (38) results in an ordinary differential equation

$$\left[\frac{\partial f(S_{\mathrm{W}})}{\partial S_{\mathrm{W}}} - c\right] S'_{\mathrm{W}} - \left[\mathrm{D}(S_{\mathrm{W}})S'_{\mathrm{W}}\right]' = 0, \tag{42}$$

where the prime $'$ denotes d/dy. Integrating (42) from a fixed y_0 to a y gives

$$S'_{\mathrm{W}}(y) = \frac{1}{\mathrm{D}(S_{\mathrm{W}}(y))}\left[f(S_{\mathrm{W}}(y)) - cS_{\mathrm{W}}(y) + c_0\right] \tag{43}$$

with the integration constant

$$c_0 = cS_{\mathrm{W}}(y_0) - f(S_{\mathrm{W}}(y_0)) + \mathrm{D}(S_{\mathrm{W}}(y_0))S'_{\mathrm{W}}(y_0). \tag{44}$$

Equation (43) describes a dynamical system with the three parameters c, c_0, and y_0.

Existence and uniqueness of solutions of Eq. (43) are guaranteed by the Picard–Lindelöf theorem (Smoller 1983; Perko 1993). Generally, the solutions are normalized (i.e., anchored translationally) by choosing y_0 such that the quantities

$$-\infty < y_0 < \infty, \tag{45a}$$

$$0 < S_{\mathrm{W}}(y_0) < 1, \tag{45b}$$

$$-\infty < S'_{\mathrm{W}}(y_0) < \infty \tag{45c}$$

are bounded away from their limiting values.

In Sect. 5 below a very different normalization (anchoring) will be used. To the best of our knowledge such an anchoring has not been used before and is specified by setting

$$y_0 = \infty, \tag{46a}$$

$$S_{\mathrm{W}}(\infty) = S_{\mathrm{W}}{}^{\mathrm{r}}, \tag{46b}$$

$$S'_{\mathrm{W}}(\infty) = 0. \tag{46c}$$

This normalization effectively eliminates the parameter y_0 from the discussion. It permits a complete and exhaustive discussion for the special class of all smooth solutions with the help of two reduced graphical representations introduced below in Sect. 5.

3.2 Dynamical System Approach

A qualitative description of the global structure of all solutions of Eq. (43) is obtained by applying a geometrical dynamical system approach (Brevdo et al. 2001; Smoller 1983). Equation (42) is transformed into a two-dimensional dynamical system

$$X' = Y, \tag{47a}$$

$$Y' = \frac{1}{\mathrm{D}(X)}\left[\left(\frac{\partial f(X)}{\partial X} - c\right)Y - \frac{\partial \mathrm{D}(X)}{\partial X}Y^2\right], \tag{47b}$$

where we rename

$$X = S_{\mathbb{W}}, \tag{48a}$$

$$Y = S'_{\mathbb{W}} \tag{48b}$$

to emphasize the mathematical structure. The set of stationary points is

$$\mathfrak{S} = \{(X, Y) \in [S_{\mathbb{W}0}, S^*_{\mathbb{W}}] \times \mathbb{R} | S_{\mathbb{W}0} < X < S^*_{\mathbb{W}} \text{ and } Y = 0\}. \tag{49}$$

The parameter $S_{\mathbb{W}0}$ was defined in Eq. (28). For imbibition processes, it denotes the saturation at which the imbibition started and hence is the smallest saturation during a process. The parameter $S^*_{\mathbb{W}}$ was defined in Eq. (8c) and denotes the maximally possible value for the water saturation.

3.3 Linearization and Stability

The stability of system (47) around the stationary points $S_0 = (X_0, 0) \in \mathfrak{S}$ is given by the eigenvalues of the linearized system

$$\begin{pmatrix} X \\ Y \end{pmatrix}' = \begin{pmatrix} 0 & 1 \\ 0 & a_{22}(X_0) \end{pmatrix} \begin{pmatrix} X - X_0 \\ Y \end{pmatrix} \tag{50}$$

with

$$a_{22}(X_0) = \frac{f'(X_0) - c}{\mathrm{D}(X_0)}. \tag{51}$$

The eigenvalues are 0 and $\mathrm{e}_1(\mathrm{X}_0) = \mathrm{a}_{22}(\mathrm{X}_0)$. The capillary function $\mathrm{D}(X)$ is a nonnegative function. The stationary points are classified as

$$S_0 \text{ is } \begin{cases} \text{stable}, & \text{if} \quad S_0 \in \mathfrak{S}_{\mathrm{r}} = \{(X_0, 0) \in \mathfrak{S} | f'(X_0) < c\}, \\ \text{unstable}, & \text{if} \quad S_0 \in \mathfrak{S}_{\ell} = \{(X_0, 0) \in \mathfrak{S} | f'(X_0) > c\}. \end{cases} \tag{52}$$

The sets $\mathfrak{S}_{\mathrm{r}}$ and $\mathfrak{S}_{\ell}$ contain the stable and unstable stationary points. The set of all stationary points is given by $\mathfrak{S} = \mathfrak{S}_{\mathrm{r}} \cup \mathfrak{S}_{\ell} \cup \mathfrak{S}_z$, where

$$\mathfrak{S}_z = \{(X_0, 0) \in \mathfrak{S} | f'(X_0) = c\} \tag{53}$$

are the stationary points with both eigenvalues equal to zero. There are no saddle points because the dynamical system has only one single nonzero eigenvalue.

3.4 Trajectories and Their Asymptotic Behavior

For fixed velocity c, we use Eq. (43) to define the trajectories in the phase portrait (X, Y) with parameter c_0 by

$$Y_{c_0}(X) = \frac{f(X) - cX + c_0}{\mathrm{D}(X)}. \tag{54}$$

The direction of the trajectories in the phase portrait (X, Y) is from left to right in the upper half plane ($Y = S'_{\mathbb{W}} > 0$) and from right to left in the lower half plane ($Y = S'_{\mathbb{W}} < 0$). In imbibition processes, only the lower half plane is of interest.

We now want to analyze the behavior of the trajectories for the limits $X \searrow S_{\mathbb{W}0}$ and $X \nearrow S^*_{\mathbb{W}}$. This is necessary because the Y-values of the trajectories go to $-\infty$ or ∞ where X goes to its maximum $S^*_{\mathbb{W}}$ or minimum $S_{\mathbb{W}0}$ because the capillary function $\mathrm{D}(X)$ vanishes there.

The behavior of the trajectories at $X \searrow S_{\mathbb{W}0}$ is determined by

$$\lim_{X \searrow S_{\mathbb{W}0}} Y_{c_0}(X) = \lim_{X \searrow S_{\mathbb{W}0}} \frac{-cX + c_0}{\mathrm{D}(X)} = \mathrm{sgn}(c_0 - c\, S_{\mathbb{W}0})\, \infty. \tag{55}$$

The trajectory $\mathcal{C}_0(X) = Y_{c\, S_{\mathbb{W}0}}(X)$ for $c_0 = c\, S_{\mathbb{W}0}$ determines the behavior at $X \searrow S_{\mathbb{W}0}$. It separates the trajectories whose Y-values tend to ∞ for $X \searrow S_{\mathbb{W}0}$ ($c_0 > c\, S_{\mathbb{W}0}$) from the ones whose Y-values tend to $-\infty$ for $X \searrow S_{\mathbb{W}0}$ ($c_0 < c\, S_{\mathbb{W}0}$). The trajectory $\mathcal{C}_0$ is therefore called separating curve.

The behavior of the trajectories at $X \nearrow S^*_{\mathbb{W}}$ is determined by

$$\lim_{X \nearrow S^*_{\mathbb{W}}} Y_{c_0}(X) = \lim_{X \nearrow S^*_{\mathbb{W}}} \frac{1 - c\, S^*_{\mathbb{W}} + c_0}{\mathrm{D}(X)} = \mathrm{sgn}(1 - c\, S^*_{\mathbb{W}} + c_0)\, \infty. \tag{56}$$

The trajectory $\mathcal{C}_1(X) = Y_{c\, S^*_{\mathbb{W}} - 1}(X)$ for $c_0 = c\, S^*_{\mathbb{W}} - 1$ determines the behavior at $X \nearrow S^*_{\mathbb{W}}$. It separates the trajectories whose Y-values tend to ∞ for $X \nearrow S^*_{\mathbb{W}}$ ($c_0 > c\, S^*_{\mathbb{W}} - 1$) from the ones whose Y-values tend to $-\infty$ for $X \nearrow S^*_{\mathbb{W}}$ ($c_0 < c\, S^*_{\mathbb{W}} - 1$). The trajectory $\mathcal{C}_0$ is also called separating curve.

The two separating curves $\mathcal{C}_0, \mathcal{C}_1$ coincide if $c = 1/(S^*_{\mathbb{W}} - S_{\mathbb{W}0})$. For smaller velocities one has $\mathcal{C}_0 > \mathcal{C}_1$ and for higher velocities one has $\mathcal{C}_0 < \mathcal{C}_1$. The behavior of the separating curves $\mathcal{C}_0, \mathcal{C}_1$ at $S_{\mathbb{W}0}, S^*_{\mathbb{W}}$ is determined by

$$\lim_{X \searrow S_{\mathbb{W}0}} \mathcal{C}_0(X) = 0, \tag{57a}$$

$$\lim_{X \searrow S_{\mathbb{W}0}} \mathcal{C}_1(X) = \begin{cases} +\infty, & \text{if} \quad c > 1/(S^*_{\mathbb{W}} - S_{\mathbb{W}0}), \\ -\infty, & \text{if} \quad c < 1/(S^*_{\mathbb{W}} - S_{\mathbb{W}0}), \end{cases} \tag{57b}$$

$$\lim_{X \nearrow S^*_{\mathbb{W}}} \mathcal{C}_0(X) = \begin{cases} +\infty, & \text{if} \quad c < 1/(S^*_{\mathbb{W}} - S_{\mathbb{W}0}), \\ -\infty, & \text{if} \quad c > 1/(S^*_{\mathbb{W}} - S_{\mathbb{W}0}), \end{cases} \tag{57c}$$

$$\lim_{X \nearrow S^*_{\mathbb{W}}} \mathcal{C}_1(X) = 0 \tag{57d}$$

and differs from their behavior in the traditional theory with Brooks and Corey parameter functions (Brevdo et al. 2001) where they diverge in each limit.

4 Results

4.1 Phase Portraits

This subsection shows phase portraits and bifurcations for the two main imbibition processes with parameters from Tables 1 and 2 and highlights the differences between the phase portraits found in Brevdo et al. (2001). The notations $S_{\mathbb{W}}, S'_{\mathbb{W}}$ instead of X, Y will be used in this section. Figure 2 shows the parameter functions. A first difference to Brevdo et al. (2001) is that the real and not the effective saturations are used. This permits to explicitly account for differences between primary and secondary imbibitions.

Similarly to Brevdo et al. (2001), there are four profile classes which are topologically different in the phase portrait. A representative example of each class is shown in Fig. 3 as

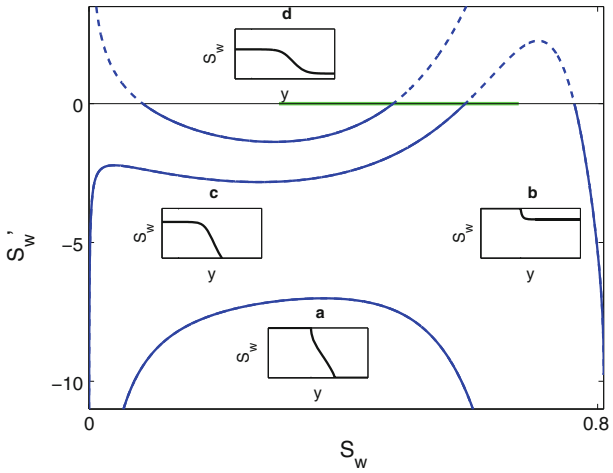

Fig. 3 For each profile class, a trajectory (*blue lines*) in the phase portrait and a saturation profile (*inlet figures*) are shown. The *green line* displays the unstable stationary points. The rest of the *line* $S'_{\mathbb{W}} = 0$ shows the stable stationary points. For imbibition processes only the lower half plane is of interest

trajectories in the phase portrait with associated saturation profiles. To study the behavior of the trajectories at points of infinity, we use the Poincaré sphere. The Poincaré sphere is the 2-unit sphere $S^2 = \{(X, Y, Z)|X^2 + Y^2 + Z^2 = 1\} \in \mathbb{R}^3$ where one gnomonically projects from the (X, Y) plane tangent to the north pole of the sphere $\{(X, Y, Z) \in \mathbb{R}^3|Z = 1\}$ to the center of this sphere (0,0,0) onto the surface of the upper half sphere $\{(X, Y, Z) \in S^2|Z \geq 0\}$. Therefore, the points at infinity on the plane are projected onto the equator of the sphere $\{(X, Y, Z) \in S^2|Z = 0\}$ [see Perko (1993, p. 267)]. In the phase portrait, homoclinic and heteroclinic orbits can be identified. A homoclinic orbit is a trajectory which connects a point with itself. A heteroclinic orbit is a trajectory which connects two different stationary points. Class (a) are homoclinic orbits connecting the point $(0, -1, 0)$ on the Poincaré sphere with itself. Class (b) are heteroclinic orbits connecting the point $(0, -1, 0)$ on the Poincaré sphere with a stable stationary point. Class (c) are heteroclinic orbits connecting an unstable stationary point with the point $(0, -1, 0)$ on the Poincaré sphere. Class (d) are heteroclinic orbits connecting an unstable stationary point with a stable stationary point.

Figure 4 displays nine phase portraits for velocities $c = 1, 1.235, 1.3, 1.37, 1.5, 1.738, 2, 2.69, 3$ for the primary imbibition. The blue lines show ordinary trajectories. The red lines show the separating curves $\mathcal{C}_0, \mathcal{C}_1$. They coincide for $c = 1.235$. The green dashed lines show the two trajectories $\mathcal{N}_1, \mathcal{N}_2$. These are defined as the trajectories that cross the stationary points with zero eigenvalues $\mathfrak{S}_z$. These two trajectories separate the trajectories which go though the unstable stationary points. Their c_0 values are denoted as $c_0(\mathcal{N}_1) > c_0(\mathcal{N}_2)$. The black lines at $S'_{\mathbb{W}} = 0$ show the stable stationary points $\mathfrak{S}_\mathrm{r}$ and the green lines show the unstable stationary points $\mathfrak{S}_\ell$. Note that a single trajectory can produce two different imbibition profiles if and only if $c_0 \in (c_0(\mathcal{N}_2), \min\{cS^*_{\mathbb{W}} - f(S^*_{\mathbb{W}}), c_0(\mathcal{N}_1)\})$.

There are four bifurcations at $c = 1.235, 1.37, 1.738, 2.69$. At $c = 1.235$ both separating curves cross each other. At $c = 1.37$ the separating curve $\mathcal{C}_0$ crosses the trajectory $\mathcal{N}_2$ and at $c = 1.738$ the separating curve $\mathcal{C}_1$ crosses the trajectory $\mathcal{N}_1$. At $c = 2.69$ the trajectories $\mathcal{N}_1$ and $\mathcal{N}_2$ coincide and for higher velocities they do not exist.

The phase portraits for secondary imbibition look qualitatively the same. The only differences are the minimal water saturation which is $S_{\mathbb{W}0} = S_{\mathbb{O}\,\mathrm{im}}$ instead of $S_{\mathbb{W}0} = 0$ and the

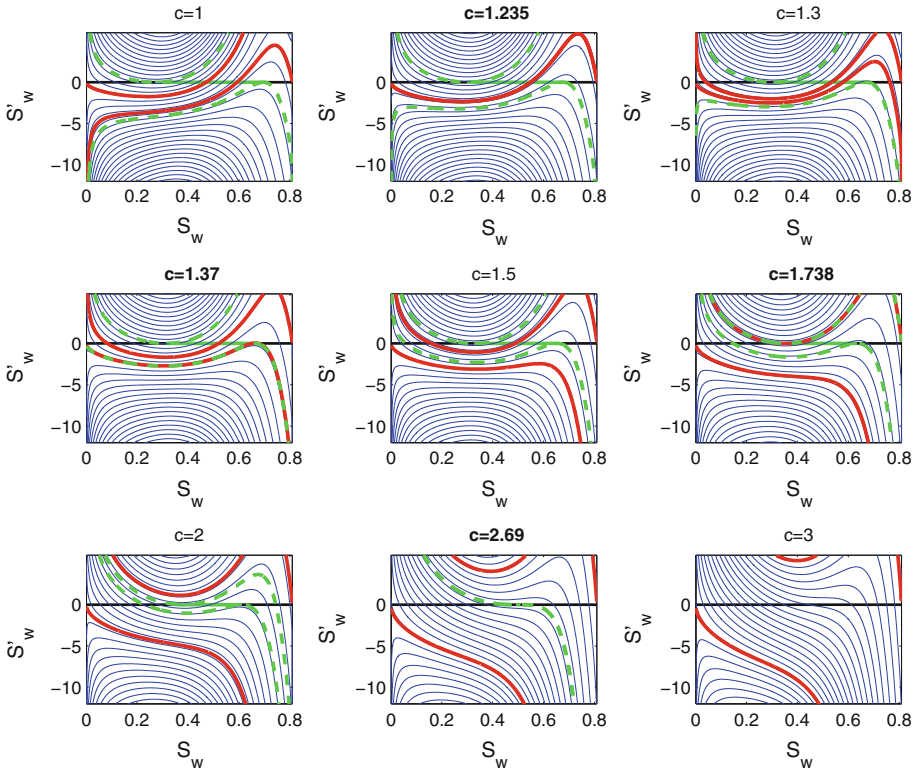

Fig. 4 Phase portraits for velocities $c = 1, 1.235, 1.3, 1.37, 1.5, 1.738, 2.69, 3$ for primary imbibition with parameters from Tables 1 and 2. The *blue lines* show ordinary trajectories and the *red lines* show the separating curves. The *dashed green lines* show trajectories which cross the stationary points with zero eigenvalues $\mathfrak{S}_z$. At $S'_{\mathbb{W}} = 0$, the *black lines* show the stable stationary points $\mathfrak{S}_\mathrm{r}$ and the *green lines* show the unstable stationary points $\mathfrak{S}_\ell$. At phase portraits with velocity $c = 1.235, 1.37, 1.738, 2.69$ bifurcations happen

bifurcations happen at velocities $c = 1.52, 1.78, 1.84, 2.9$ instead of $c = 1.235, 1.37, 1.738, 2.69$.

In contrast to (Brevdo et al. 2001) smooth profiles of class (d) are found for the right boundary condition $S^\mathrm{r}_{\mathbb{W}} = 0$ with $\lim_{y\to\infty} S_{\mathbb{W}}(y) = 0$. These profiles are produced by the separating curve $\mathcal{C}_0$ in the phase portrait. For Brooks and Corey parameterizations, profiles where the right boundary condition is $S^\mathrm{r}_{\mathbb{W}} = 0$ and therefore $\lim_{y\to\infty} S_{\mathbb{W}}(y) = 0$ belong to class (c) and hence are not smooth everywhere. The reason for this difference lies in the different behavior of the capillary function. The derivative of the capillary function $\mathrm{D}'(S_{\mathbb{W}})$ diverges where for Brooks and Corey it goes to zero as the water saturation reaches its minimum.

4.2 Saturation Profiles

This subsection shows saturation profiles for primary and secondary imbibition processes with parameters from Tables 1 and 2 and highlights the differences to the saturation profiles found in Brevdo et al. (2001).

Figure 5 shows eight profiles. The upper four represent primary imbibition processes and the lower four secondary imbibition processes. The first column shows profiles of class (a),

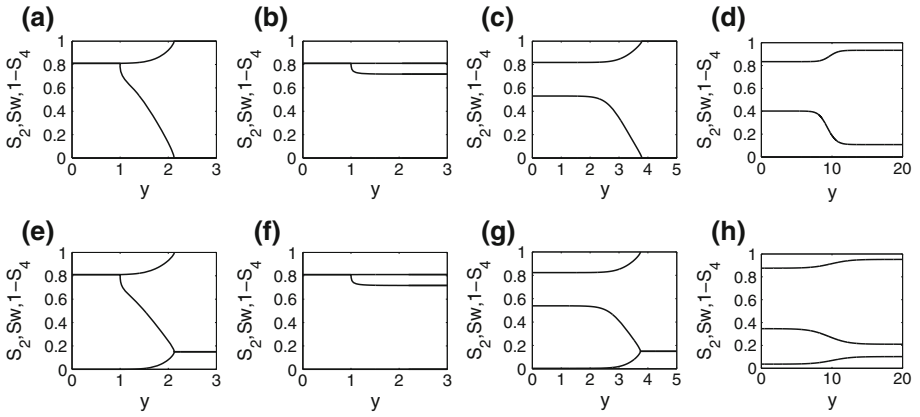

Fig. 5 Saturation profiles for primary (**a**–**d**) and secondary (**e**–**h**) imbibition of all four different profile classes. The velocity is the same $c = 1$ in all subfigures, only the c_0 value varies

Table 3 Velocities, c_0 values, boundary saturations, and profile classes for the Figs. 5 and 6

Figures	c	c_0	$S^{\ell}_{\mathbb{W}}$	$S^{\mathrm{r}}_{\mathbb{W}}$	S^{ℓ}_2	S^{r}_2	S^{ℓ}_4	S^{r}_4	Profile class
5a	1	−0.3	0.81	0	0	0	0.19	0	(a)
5e	1	−0.3	0.81	0.15	0	0.15	0.19	0	(a)
5b	1	−0.25	0.81	0.72	0	0	0.19	0.19	(b)
5f	1	−0.25	0.81	0.72	0	0	0.19	0.19	(b)
5c	1	−0.1	0.53	0	0	0	0.18	0	(c)
5g	1	−0.1	0.54	0.15	0.01	0.15	0.18	0	(c)
5d	1	0.1	0.40	0.11	0	0	0.17	0.07	(d)
5h	1	0.2	0.35	0.21	0.04	0.10	0.12	0.05	(d)
6a	1.37	0	0.66	0	0	0	0.19	0	(d)
6b	1.78	0.26	0.64	0.15	0	0.15	0.19	0	(d)

the second column of class (b), the third column of class (c) and the fourth column of class (d). All waves have the same velocity $c = 1$. They differ in their c_0 values and therefore in their boundary conditions (see Table 3).

Figure 5a displays a profile of class (a) for primary imbibition. A water front imbibes a medium completely filled with percolating oil. The water saturation increases to its maximal value $1 - S_{\mathbb{O}\,\mathrm{im}}$ and a maximal amount of nonpercolating oil is produced. Fig. 5e shows a profile of class (a) for secondary imbibition. A water front imbibes a medium which contains a maximal amount of nonpercolating water but no percolating water. The water saturation increases to its maximal value $1 - S_{\mathbb{O}\,\mathrm{im}}$, a maximal amount of nonpercolating oil is produced and all the nonpercolating water becomes percolating.

Figure 5b contains a profile of class (b) for primary imbibition. A water front imbibes a medium filled with maximal amount of nonpercolating oil and to 72 % with percolating water. The water saturation increases to its maximal value $1 - S_{\mathbb{O}\,\mathrm{im}}$ and the nonpercolating phases do not change. Figure 5f contains a profile of class (b) for secondary imbibition. There is almost no difference between primary and secondary imbibition because the nonpercolating phases are constant and identical for $S_{\mathbb{W}} \in (0.7, 0.81)$, see Fig. 1a.

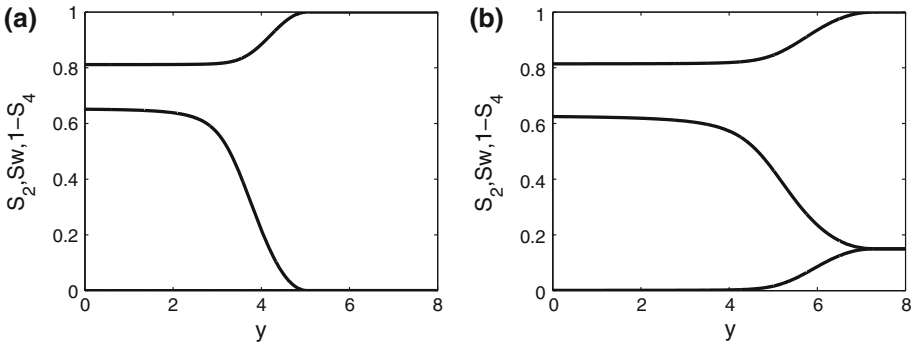

Fig. 6 Maximal saturation profiles of class (d) for primary (**a**) and secondary (**b**) imbibition

Figure 5c contains a profile of class (c) for primary imbibition. A water front imbibes a medium completely filled with percolating oil. The water saturation increases to 53 % and nonpercolating oil is produced up to a value of 18 %. Figure 5g contains a profile of class (c) for secondary imbibition. A water front imbibes a medium filled with maximal percolating oil and maximal nonpercolating water. The water saturation increases to 54 %, nonpercolating oil is produced up to a value of 18 % and almost all nonpercolating water becomes percolating.

Figure 5d contains a profile of class (d) for primary imbibition. A water front imbibes a medium filled with 82 % percolating oil, 7 % nonpercolating oil and 11 % percolating water. The water saturation increases to 40 % and nonpercolating oil is produced up to a value of 17 %. Figure 5h contains a profile of class (d) for secondary imbibition. A water front imbibes a medium filled with 74 % percolating oil, 5 % nonpercolating oil, 11 % percolating water and 10 % nonpercolating water. The water saturation increases to 35 %, nonpercolating oil is produced up to a value of 12 % and up to 4 % all nonpercolating water becomes percolating.

Figure 6 shows the smooth traveling waves with the largest possible difference between the left and the right saturation for the primary and secondary imbibition which correspond to the separating curve C_0 in the phase portrait. Figure 6a displays a water front imbibing a medium completely filled with percolating oil. The water saturation increases to 66 % and nonpercolating oil is produced to its maximal value 19 %. The velocity is $c = 1.37$. Figure 6b contains a water front imbibing a medium filled with 85 % percolating oil and 15 % nonpercolating water. The water saturation increases to 64 %, nonpercolating oil is produced to its maximal value 19 % and all nonpercolating water becomes percolating. The velocity is $c = 1.78$. So the velocity is significantly larger for the secondary than for the primary imbibition. Furthermore and quite surprisingly the water saturation behind the front is larger for the primary than for the secondary imbibition although already 15 % of water is initially present during the secondary imbibition. This elucidates the importance to distinguish between the primary and secondary imbibition and including percolating and nonpercolating phases which was not the case in Brevdo et al. (2001).

5 Two Reduced Graphical Representations of all Differentiable Traveling Waves

From here on, the discussion is restricted to traveling waves of class (d). It is the only class with profiles that are everywhere smooth. Because of this property, many authors Cueto-Felgueroso and Juanes (2009), Gilding and Kersner (2001), Volpert et al. (1994) limit their

studies to class (d) beforehand. We follow this practice here. The limitation to smooth solutions allows to effectively eliminate the parameter y_0 from the discussion by setting $y_0 = \infty$ and changing the normalization from Eqs. (45) to (46).

This section discusses two reduced representations of all smooth traveling waves. The reduced representations enable us to plot all global information of smooth traveling waves—the wave velocity c and the boundary conditions $(S_{\mathbb{W}}^{\ell}, S_{\mathbb{W}}^{\mathrm{r}})$—in one single figure. Without this representation many phase portraits are necessary to illustrate all global information. This exacerbates a quantitative comparison of the solution space $(c, S_{\mathbb{W}}^{\ell}, S_{\mathbb{W}}^{\mathrm{r}})$ of traveling waves for different models or model parameters. With the reduced representations, the difference between two models can be assessed through the comparison of two figures. Important information such as the maximal traveling wave height or the maximal velocity can be very easily read off one of these figures.

In this article, these representations are mainly used to illustrate the differences between secondary and primary imbibition of one parameter set of the generalized model assuming immobile nonpercolating phases. But the reduced representations can be applied to other models with flow functions, even if they are non-monotonic. Moreover, these representations can be used for the Buckley–Leverett limit and therefore for shock waves because traveling waves and shock waves are connected through the vanishing viscosity limit (Duijn et al. 2007). The ideas for these representations are partially borrowed from the standard analysis of shock waves of the Buckley–Leverett limit.

5.1 Representation 1: The Integration Constant c_0

The first reduced representation uses the established picture (Welge 1952) that a shock wave in the Buckley–Leverett limit can be represented as a straight line in the flow function figure. This line will be called traveling wave line in this article. Its slope represents the wave velocity. The y intercept is the negative of the integration constant of the traveling wave formulation. Its intersections with the flow function are the possible boundary values. Segments of the traveling wave line having higher values than the flow function are imbibition shocks and segments of the traveling wave line having lower values than the flow function are drainage shocks. The integration constant can now be written as a function of one possible boundary condition and the velocity. The sign of the derivative of the integration constant function in respect to the boundary condition tells us whether the boundary condition is left- or right-sided. Plotting the integration constant function and using the sign of its derivative, represents all global information.

5.1.1 Method

Using the normalization (46c) and the fact that for smooth solutions of class (d) $S'_{\mathbb{W}}(-\infty) = 0$ holds at the left limit one finds

$$cS_{\mathbb{W}}^{\ell} - c_0 = f(S_{\mathbb{W}}^{\ell}), \tag{58a}$$

$$cS_{\mathbb{W}}^{\mathrm{r}} - c_0 = f(S_{\mathbb{W}}^{\mathrm{r}}), \tag{58b}$$

from Eq. (44). For saturations excluding the bounding saturations the capillary function is finite and Eq. (44) requires

$$cS_{\mathbb{W}} - c_0 = f(S_{\mathbb{W}}) \Leftrightarrow S'_{\mathbb{W}} = 0. \tag{59}$$

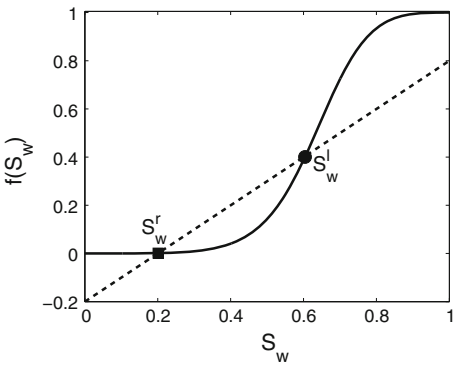

Fig. 7 $\mathcal{L}(S_{\mathbb{W}}) = S_{\mathbb{W}} - 0.2$ (*dashed line*), $f(S_{\mathbb{W}})$ (*solid line*) and their intersection points at $S^{\mathrm{r}}_{\mathbb{W}}$ (*square*) and $S^{\ell}_{\mathbb{W}}$ (*circle*)

This permits the definition of a function c_0 that depends on velocity and the stationary points

$$c_0(S_{\mathbb{W}}, c) = cS_{\mathbb{W}} - f(S_{\mathbb{W}}). \tag{60}$$

It couples the boundary saturations $S^{\ell}_{\mathbb{W}}$, $S^{\mathrm{r}}_{\mathbb{W}}$ and the velocity c. The left-hand side of Eq. (59) describes a line $\mathcal{L}(S_{\mathbb{W}})$ with variable $S_{\mathbb{W}}$, slope c and y intercept $-c_0$. The right-hand side describes the fractional flow function $f(S_{\mathbb{W}})$. Whenever $\mathcal{L}(S_{\mathbb{W}})$ and $f(S_{\mathbb{W}})$ intersect, then the corresponding $S_{\mathbb{W}}$ is a stationary saturation. Its stability is given by

$$\frac{\partial}{\partial S_{\mathbb{W}}} c_0(S_{\mathbb{W}}, c) = c - f'(S_{\mathbb{W}}) \begin{cases} < 0 & S_{\mathbb{W}} \text{ is stable,} \\ > 0 & S_{\mathbb{W}} \text{ is unstable.} \end{cases} \tag{61}$$

This means that the intersection point is a stable stationary point and therefore a possible $S^{\mathrm{r}}_{\mathbb{W}}$ if the slope of $\mathcal{L}$ is larger than the slope of f, and an unstable stationary point and therefore a possible $S^{\ell}_{\mathbb{W}}$ if the slope of $\mathcal{L}$ is smaller than the slope of f. Therefore, the line $\mathcal{L}$ has higher values than the fractional flow function for all saturations between $S^{\mathrm{r}}_{\mathbb{W}}$ and $S^{\ell}_{\mathbb{W}}$. Figure 7 shows an example for $c = 1$ and $c_0 = 0.2$. The corresponding saturations are $S^{\mathrm{r}}_{\mathbb{W}} = 0.19$ and $S^{\ell}_{\mathbb{W}} = 0.63$.

5.1.2 Results

Figure 8 shows the function $c_0(S_{\mathbb{W}}, c)$ as a color plot for primary and secondary imbibition. On the lines E, A, F the derivative $\partial c_0(S_{\mathbb{W}}, c)/\partial S_{\mathbb{W}}$ is zero, in between these lines the derivative is negative, outside it is positive. Therefore, in the region bounded by these lines possible $S^{\ell}_{\mathbb{W}}$ are located, outside possible $S^{\mathrm{r}}_{\mathbb{W}}$ can be found. There is a particular traveling wave with global information (c, $S^{\ell}_{\mathbb{W}}$, $S^{\mathrm{r}}_{\mathbb{W}}$) if and only if there are two points on a horizontal line (for a fixed velocity c), one point $S^{\ell}_{\mathbb{W}}$ on the region bounded by the lines E, A , F and one point $S^{\mathrm{r}}_{\mathbb{W}}$ outside this region, with the same color (the same c_0-value). This is only the case for points in the shaded regions. Hence, the horizontal shaded region displays all possible $S^{\ell}_{\mathbb{W}}$ and the vertical shaded region displays all possible $S^{\mathrm{r}}_{\mathbb{W}}$. Points lying between C, F and the $S_{\mathbb{W}}-$axis could serve as possible $S^{\ell}_{\mathbb{W}}$ but their traveling wave lines do not have a second intersection point of $\mathcal{L}$ and f which could give a possible $S^{\mathrm{r}}_{\mathbb{W}}$. Points lying outside B, A, F could serve as possible $S^{\mathrm{r}}_{\mathbb{W}}$ but their traveling wave lines do not have a second intersection point of $\mathcal{L}$ and f which could give a possible $S^{\ell}_{\mathbb{W}}$.

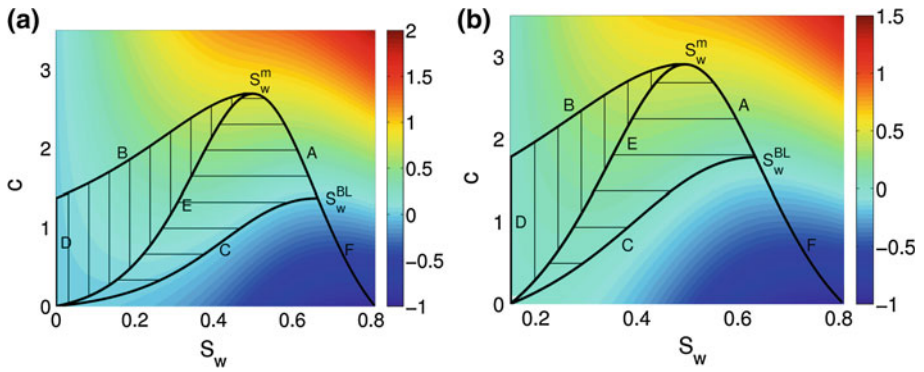

Fig. 8 Reduced representations of all differentiable traveling waves. The function $c_0(S_\mathrm{W}, c)$ as a color plot for primary (**a**) and secondary (**b**) imbibition. On the lines E, A, F the derivative $\partial c_0(S_\mathrm{W}, c)/\partial S_\mathrm{W}$ is zero, in between these lines the derivative is negative, outside it is positive. Therefore, in the region bounded by these lines possible S_W^ℓ are located, outside possible S_W^r can be found. There is a particular traveling wave for $(c, S_\mathrm{W}^\ell, S_\mathrm{W}^\mathrm{r})$ if and only if there are two points on a *horizontal line* (for a fixed velocity c), one point S_W^ℓ on the region bounded by the *lines E, A , F* and one point S_W^r outside this region, with the same color (the same c_0 value). This is only the case for the points in the *shaded* regions. Hence, the *horizontal shaded* region displays all possible S_W^ℓ and the *vertical shaded* region displays all possible S_W^r

Important information about the solution space of traveling waves, such as the maximal velocity or maximal saturation, can be easily identified in Fig. 8. The maximal velocity of a traveling wave is $c^\mathrm{max} = \max_{S_\mathrm{W}\in(0,1)} f'(S_\mathrm{W})$ and its corresponding saturation S_W^m is the only inflection point of $f(S_\mathrm{W})$. The maximal left-sided boundary saturation is $S_\mathrm{W}^\mathrm{BL} = \{S_\mathrm{W} | c^\mathrm{BL} = f(S_\mathrm{W})/(S_\mathrm{W} - S_{\mathrm{W}0})\text{maximal}\}$. The saturation S_W^BL is the left-sided limit of a maximal Buckley–Leverett shock (Welge 1952). One can see in Fig. 8 that higher velocities are possible for the secondary imbibition. The saturations S_W^m for the fastest wave are however identical. The maximal saturation S_W^BL is 2 % lower for a secondary imbibition although there is already 15 % initially present.

There are three boundary regimes

(i) Traveling waves connecting C and D with boundary saturations $(S_\mathrm{W}^\ell, S_\mathrm{W}^\mathrm{r}) \in \{(S_\mathrm{W}^\ell, 0) | S_\mathrm{W}^\ell \in (0, S_\mathrm{W}^\mathrm{BL})\}$ and velocities $c = f'(S_\mathrm{W}^\ell)/S_\mathrm{W}^\ell$. These are the maximal imbibition waves in a completely dry porous medium.

(ii) Traveling waves connecting A and B with boundary saturations $(S_\mathrm{W}^\ell, S_\mathrm{W}^\mathrm{r}) \in \{(S_\mathrm{W}^\ell, S_\mathrm{W}^\mathrm{r}) | S_\mathrm{W}^\ell \in (S_\mathrm{W}^\mathrm{m}, S_\mathrm{W}^\mathrm{BL}) \cup S_\mathrm{W}^\mathrm{r} \in (0, S_\mathrm{W}^\mathrm{m})\}$ and velocities $c = (f(S_\mathrm{W}^\ell) - f(S_\mathrm{W}^\mathrm{r}))/(S_\mathrm{W}^\ell - S_\mathrm{W}^\mathrm{r})$. These are imbibition waves with the maximal saturation difference into a porous medium with an initial saturation S_W^r. This is the Welge construction (Welge 1952) for given initial saturation S_W^r.

(iii) Line E represents traveling waves with $S_\mathrm{W}^\ell = S_\mathrm{W}^\mathrm{r} \in (0, S_\mathrm{W}^\mathrm{m})$ and velocities $c = f'(S_\mathrm{W}^\ell)$. These are the waves with constant saturations.

Figure 9 shows examples for traveling wave lines representing traveling waves of type (i) and (ii). In Fig. 9a, the profiles range from the minimal wave $S_\mathrm{W}^\ell = S_\mathrm{W}^\mathrm{r} = c = 0$ up to the maximal wave $S_\mathrm{W}^\ell = S_\mathrm{W}^\mathrm{BL}$, $S_\mathrm{W}^\mathrm{r} = 0$, $c = c^\mathrm{BL}$. In Fig. 9b, the profiles span the fastest wave $S_\mathrm{W}^\ell = S_\mathrm{W}^\mathrm{r} = S_\mathrm{W}^\mathrm{m}$, $c = c^\mathrm{max}$ and the maximal wave $S_\mathrm{W}^\ell = S_\mathrm{W}^\mathrm{BL}$, $S_\mathrm{W}^\mathrm{r} = 0$, $c = c^\mathrm{BL}$.

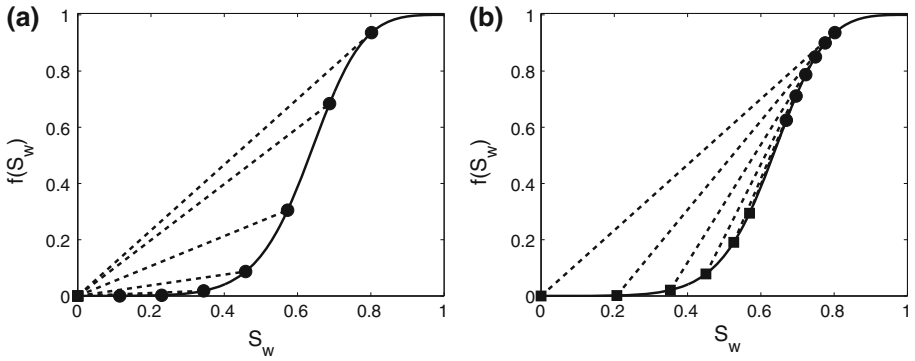

Fig. 9 Examples for traveling wave lines $\mathcal{L}(S_{\mathbb{W}}) = S_{\mathbb{W}} - 0.2$ (*dashed lines*) and their intersections with the flow function (*solid line*) at $S_{\mathbb{W}}^{\mathrm{r}}$ (*square*) and $S_{\mathbb{W}}^{\ell}$ (*circle*) for traveling waves of type (i) in subfigure (**a**) and for type (ii) in subfigure (**b**)

5.2 Representation 2: The shock speed c

The second representation uses the Rankine–Hugoniot condition to plot the functionality between the velocity and the two boundary conditions. In addition, the Rankine–Hugoniot condition can be defined as a function of the nonpercolating boundary saturations because the nonpercolating phases are bijective functions of the water saturation for fixed $(S_{20}, S_{40}, S_{\mathbb{W}0})$. This leads to some interesting insights about nonpercolating phases and their influence on the velocity of a traveling wave.

5.2.1 Method

Another approach uses $S'_{\mathbb{W}}(\pm\infty) = 0$ and Eq. (58) to obtain the Rankine–Hugoniot condition

$$c(S_{\mathbb{W}}^{\ell}, S_{\mathbb{W}}^{\mathrm{r}}) = \frac{f(S_{\mathbb{W}}^{\ell}) - f(S_{\mathbb{W}}^{\mathrm{r}})}{S_{\mathbb{W}}^{\ell} - S_{\mathbb{W}}^{\mathrm{r}}} \tag{62}$$

for the velocity of a shock wave. The shock velocity is a function of the nonpercolating boundary saturations

$$c(S_2^{\ell}, S_2^{\mathrm{r}}) = c({S_2}^{-1}(S_2^{\ell}), \quad {S_2}^{-1}(S_2^{\mathrm{r}})) = c(S_{\mathbb{W}}^{\ell}, S_{\mathbb{W}}^{\mathrm{r}}), \tag{63a}$$

$$c(S_4^{\ell}, S_4^{\mathrm{r}}) = c({S_4}^{-1}(S_4^{\ell}), \quad {S_4}^{-1}(S_4^{\mathrm{r}})) = c(S_{\mathbb{W}}^{\ell}, S_{\mathbb{W}}^{\mathrm{r}}), \tag{63b}$$

where the S_2^{-1} and S_4^{-1} denote inverse functions with respect to the water saturation $S_{\mathbb{W}}$ because the nonpercolating phases are bijective functions of the water saturation for fixed $(S_{20}, S_{40}, S_{\mathbb{W}0})$.

5.2.2 Results

Figure 10 shows color plots for $c(S_{\mathbb{W}}^{\ell}, S_{\mathbb{W}}^{\mathrm{r}}), c(S_2^{\ell}, S_2^{\mathrm{r}}), c(S_4^{\ell}, S_4^{\mathrm{r}})$ for the primary and secondary imbibition. Each colored point represents a traveling wave with corresponding velocity and boundary saturations. The three edges of the colored region stand for the three boundary regimes defined in Sect. 5.1.2. The corners stand for the wave with constant saturation $S_{\mathbb{W}} = 0$, for the fastest wave with constant saturation $S_{\mathbb{W}}^{\mathrm{m}}$ and for the imbibition wave into a

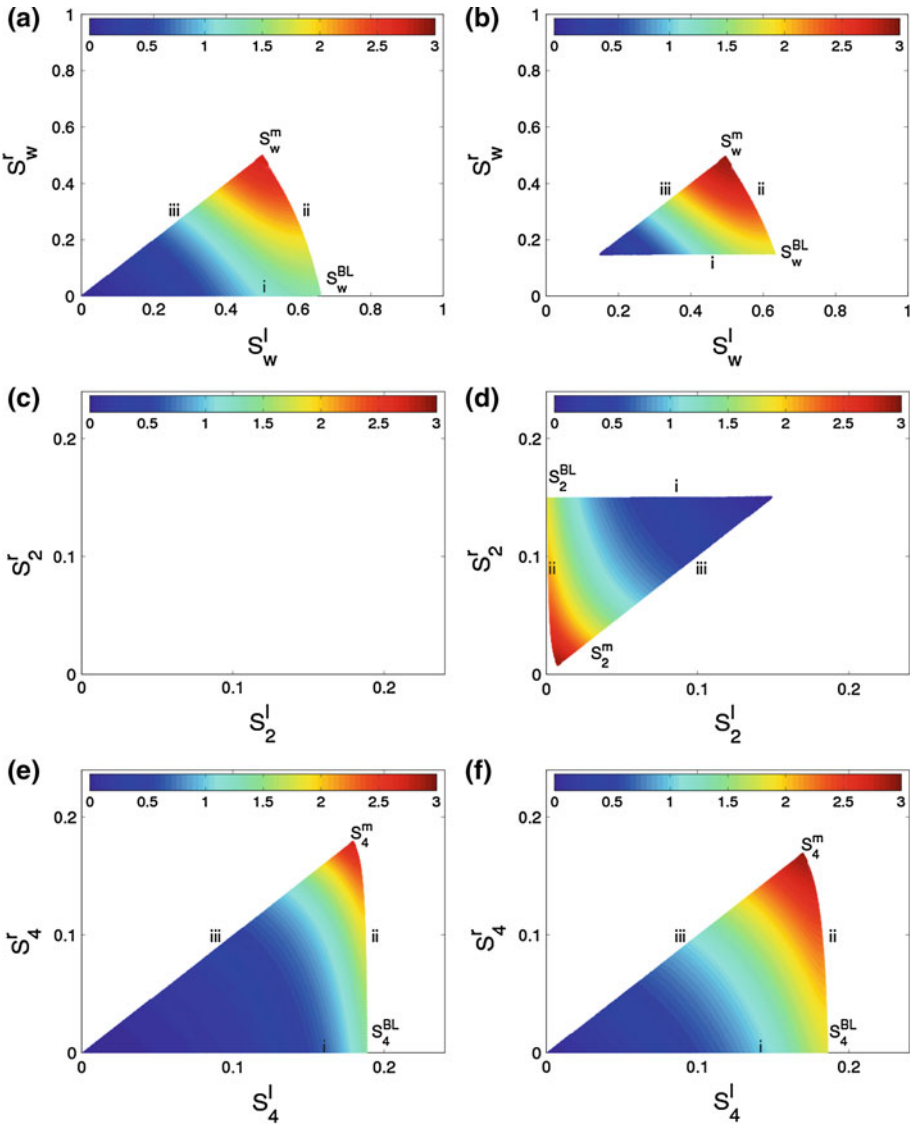

Fig. 10 *Color plots* for $c(S_{\mathbb{W}}^{\ell}, S_{\mathbb{W}}^{\mathrm{r}})$ for the primary (**a**) and secondary (**b**) imbibition, for $c(S_2^{\ell}, S_2^{\mathrm{r}})$ for the primary (**c**) and secondary (**d**) imbibition, and for $c(S_4^{\ell}, S_4^{\mathrm{r}})$ for the primary (**e**) and secondary (**f**) imbibition. Each *colored point* represents a traveling wave with corresponding velocity and boundary saturations. The three edges of the *colored region* stand for the three boundary regimes. The corners stand for the wave with constant saturation $S_{\mathbb{W}} = 0$, for the fastest wave with constant saturation $S_{\mathbb{W}}^{\mathrm{m}}$ and for the imbibition wave into a dry porous medium with maximal left-sided saturation $S_{\mathbb{W}}^{\mathrm{BL}}$

dry porous medium with maximal left-sided saturation $S_{\mathbb{W}}^{\mathrm{BL}}$. Small differences in the saturations and bigger differences in the velocities are visible. These differences cannot be seen in the traditional model where one uses effective saturations.

Equation (63) allows to study the behavior of the nonpercolating phases. Figure 10c does not show any color contours because there is no initial nonpercolating water $S_2^{\mathrm{r}} = 0$ in a

primary imbibition process and during an imbibition process nonpercolating water is not produced $S_2^\ell = 0$. For the secondary imbibition in Fig. 10d the velocities increase if the nonpercolating water saturations behind the front are minimal. The velocities increase for given nonpercolating water saturations behind the front with decreasing initial nonpercolating water saturations. Consequently, we observe that larger differences in nonpercolating water saturation lead to smaller velocities. Higher ratios between nonpercolating and percolating water lead to slower velocities. From a physical point of view this is obvious because nonpercolating phases are assumed to be immobile and these fluid parts can only be mobilized by coalescence with the percolating phase. Therefore, the mass exchange reduces the velocity. A small amount of nonpercolating water, which remains immobile, increases the maximal velocity because the maximal velocity is 30 % higher for secondary imbibition as compared to primary imbibition. We assume that this immobile nonpercolating water occupies pore volumes which have very low conductance leading to a higher overall conductance for the porous medium.

In Fig. 10e, f, the behavior of the nonpercolating oil does not differ qualitatively between primary and secondary imbibition. It also shows similarities to the behavior of the water saturation which displays the correlation between water and nonpercolating oil due to the mass exchange term. An increasing water saturation leads to an increasing nonpercolating oil saturation due to break up. The velocities increase for given initial nonpercolating oil saturations if the nonpercolating saturations behind the front increase. For given nonpercolating oil saturations behind the front velocities increase if the initial nonpercolating saturations increase. A high presence of immobile nonpercolating oil occupying pore volume which has low conductance leads to a higher overall conductance for the porous medium.

6 Conclusion

This paper has computed traveling wave solutions of a recent generalized theory for macroscopic capillarity when it can be assumed that the nonpercolating phases are immobile. Only primary and secondary imbibition processes were considered here, but drainage processes can be studied along the same lines. The solutions have been compared to traveling wave solutions of the traditional theory and significant differences were found, because the generalized theory accounts explicitly for nonpercolating and immobile fluid parts. Breakup and coalescence slow down the front, but depending on the parameters a small amount of nonpercolating immobile fluids can also lead to higher velocity. Methodically, the complete analysis of smooth solutions was based on two novel graphical representations of the solution space that may be generalized to other solution classes. The reduced representation combines the wave speed, the boundary data and the integration constant. It simplifies the comparison between different models and provides important information, such as the maximal velocity or maximal saturation at the inlet. It can also be used to discuss shock fronts and the hyperbolic limit.

Acknowledgments The authors gratefully acknowledge financial support from the Deutsche Forschungsgemeinschaft (DFG) within the International Research and Training Group on Nonlinearities and Upscaling in Porous Media (the NUPUS project) and fruitful discussions with Paul Zegeling.

References

Abrams, A.: Influence of fluid viscosity, interfacial-tension, and flow velocity on residual oil saturation feft by waterflood. Soc. Petroleum Eng. J. **15**(5), 437–447 (1975)

Avraam, D., Payatakes, A.: Generalized relative permeability coefficients during steady-state two-phase flow in porous media, and correlation with the flow mechanisms. Transp. Porous Media **20**, 135–168 (1995)

Avraam, D., Payatakes, A.: Flow mechanisms, relative permeabilities, and coupling effects in steady-state two-phase flow through porous media, the case of strong wettability. Ind. Eng. Chem. Res. **38**(3), 778–786 (1999)

Bear, J.: Dynamics of Fluids in Porous Media. Dover Publications, New York (1972)

Bear, J., Braester, C., Menier, P.C.: Effective and relative permeabilities of anisotropic porous media. Transp. Porous Media **2**, 301–316 (1987)

Brevdo, L., Helmig, R., Haragus-Courcelle, M., Kirchgässner, K.: Permanent fronts in two-phase flows in a porous medium. Transp. Porous Media **44**, 507–537 (2001)

Bryant, S.L., Blunt, M.J.: Prediction of relative permeability in simple porous media. Phys. Rev. A **46**(4), 2004–2011 (1992)

Collins, R.: Flow of Fluids Through Porous Materials. Reinhold Publishing Corporation, New York (1961)

Cueto-Felgueroso, L., Juanes, R.: Stability analysis of a phase-field model of gravity-driven unsaturated flow through porous media. Phys. Rev. E (Statistical, Nonlinear, and Soft Matter Physics) **79**(3), 036301 (2009)

De Marsily, G.: Quantitative Hydrogeology-Groundwater Hydrology for Engineers. Academic Press, Orlando (1986)

de Wiest, R.: Flow Through Porous Media. Academic Press, New York (1969)

Dias, M.M., Payatakes, A.C.: Network models for two-phase flow in porous media part 1. Immiscible microdisplacement of non-wetting fluids. J. Fluid Mech. **164**(1), 305–336 (1986)

Doster, F.: Die bedeutung perkolierender und nichtperkolierender phasen bei mehrphasenströmungen in porösen medien auf laborskala. Ph.D. thesis, Universität Stuttgart, Holzgartenstr. 16, 70174 Stuttgart (2011)

Doster, F., Hilfer, R.: Generalized Buckley–Leverett theory for two phase flow in porous media. New J. Phys. **13**, 123,030 (2011)

Doster, F., Hönig, O., Hilfer, R.: Horizontal flow and capillarity-driven redistribution in porous media. Phys. Rev. E **86**(1), 016,317 (2012)

Doster, F., Zegeling, P.A., Hilfer, R.: Numerical solutions of a generalized theory for macroscopic capillarity. Phys. Rev. E **81**(3), 036307 (2010)

Dullien, F.: Porous Media: Fluid Transport and Pore Structure, 2nd edn. Academic Press, San Diego (1992)

Ferer, M., Ji, C., Bromhal, G., Cook, J., Ahmadi, G., Smith, D.: Crossover from capillary fingering to viscous fingering for immiscible unstable flow: experiment and modeling. Phys. Rev. E **70**(1), 16,303 (2004)

Gilding, B., Kersner, R. Travelling waves in nonlinear diffusion–convection-reaction. Memorandum 1585, Department of Applied Mathematics, University of Twente, Enschede (2001)

Helmig, R.: Multiphase Flow and Transport Processes in the Subsurface. Springer, Berlin (1997)

Hilfer, R.: Macroscopic equations of motion for two-phase flow in porous media. Phys. Rev. A **58**, 2090 (1998)

Hilfer, R.: Capillary pressure, hysteresis and residual saturation in porous media. Physica A **359**, 119 (2006)

Hilfer, R.: Macroscopic capillarity and hysteresis for flow in porous media. Phys. Rev. E **73**, 016,307 (2006)

Hilfer, R.: Macroscopic capillarity without a constitutive capillary pressure function. Physica A **371**, 209–225 (2006)

Hilfer, R., Doster, F.: Percolation as a basic concept for macroscopic capillarity. Transp. Porous Media **82**(3), 507–519 (2010)

Hilfer, R., Oeren, P.: Dimensional analysis of pore scale and field scale immiscible displacement. Transp. Porous Media **22**, 53–72 (1996)

Jamin, J.: Notes about equilibrium and flow of fluids in porous body. Acad. Sci. **50**, 172 (1860)

Perko, L.: Differential Equations and Dynamical Systems. Springer, New York (1993)

Scheidegger, A.E.: The Physics of Flow through Porous Media. University of Toronto Press, Toronto (1957)

Smoller, J.: Shock Waves and Reaction–Diffusion Equations, 2nd edn. Springer, New York (1983)

Taber, J.: Dynamic and static forces required to remove a discontinuous oil phase from porous media containing both oil and water. Soc. Petroleum Eng. J. **9**(1), 3 (1969)

van Duijn, C.J., Peletier, L.A., Pop, I.S.: A new class of entropy solutions of the Buckley–Leverett equation. SIAM J. Math. Anal. **39**(2), 507–536 (2007)

van Dijke, M., Sorbie, K.: Pore-scale network model for three-phase flow in mixed-wet porous media. Phys. Rev. E **66**(4), 46,302 (2002)

Volpert, A.I., Volpert, V.A., Volpert, V.A.: Traveling Wave Solutions of Parabolic Systems. Translations of Mathematical Monographs, p. 448. American Mathematical Society, Providence (1994)

Welge, H.J.: A simplified method for computing oil recovery by gas or water drive. AIME Trans. **195**, 99–108 (1952)
Wyckoff, R.D., Botset, H.G.: The flow of gas–liquid mixtures through unconsolidated sands. Physics **7**(9), 325–345 (1936)